ISSN 1070-3284, Russian Journal of Coordination Chemistry, 2023, Vol. 49, No. 7, pp. 420–428. © Pleiades Publishing, Ltd., 2023.
Russian Text © The Author(s), 2023, published in Koordinatsionnaya Khimiya, 2023, Vol. 49, No. 7, pp. 412–421.

Heteroleptic Zinc Catecholate Complexes with N-Donor Ligands

A. V. Maleeva[a], *, O. Yu. Trofimova[a], I. A. Yakushev[b], R. R. Aysin[c], and A. V. Piskunov[a], **

[a] *Razuvaev Institute of Organometallic Chemistry, Russian Academy of Sciences, Nizhny Novgorod, Russia*
[b] *Kurnakov Institute of General and Inorganic Chemistry, Russian Academy of Sciences, Moscow, Russia*
[c] *Nesmeyanov Institute of Organoelement Compounds, Russian Academy of Sciences, Moscow, Russia*
**e-mail: arina@iomc.ras.ru*
***e-mail: pial@iomc.ras.ru*

Received December 15, 2022; revised January 11, 2023; accepted January 12, 2023

Abstract—New heteroleptic zinc catecholate complexes based on 3,6-di-*tert*-butyl-*o*-benzoquinone and containing metal-coordinated N-donor ligands (2,2'-bipyridine and phenanthroline) were prepared by ligand exchange. According to X-ray diffraction data, both complexes were dimers with multiple intermolecular π–π interactions between the aromatic moieties of neighboring molecules (CCDC nos. 2222704 (**I**), 2222705 (**II**)). The electronic transmission spectra of crystalline samples of **I** and **II** and their solutions show broad absorption bands in the visible region with a maximum at about 500 nm.

Keywords: redox-active ligand, *o*-quinone, charge transfer, zinc, X-ray diffraction, electronic spectroscopy
DOI: 10.1134/S1070328423600134

INTRODUCTION

The interest in LL'CT compounds (LL'CT is ligand-to-ligand charge transfer) as photo-electrochromic materials capable of switching their photophysical characteristics under the action of controlling radiation or electric field has markedly increased in recent years [1]. Materials that absorb in the near-IR region are particularly important. They are based on conjugated organic molecules and aggregates [2], polymers [3], inorganic materials such as quantum dots [4], perovskites [5], and donor-acceptor metal complexes [6–11]. The last-mentioned class of compounds deserves special attention because of the large diversity of redox-active organic ligands. This enables fine tuning of the electronic properties of compounds by methods of coordination chemistry. Promising ligand systems for constructing metal derivatives of this type are bipyridines and their analogues [12] and double reduced o-quinones (catecholates) [13–17] used as acceptor and donor groups, respectively. By upgrading and functionalizing donors and acceptors, it is possible to change the positions of frontier orbitals in the synthesized metal complexes and thus to vary their optical properties over a broad range.

The vast majority of the currently known LL'CT complexes were obtained from transition metals. Metals actively studied for this purpose include nickel [18–28], cobalt [22, 28, 29], copper [20, 28], manganese [22, 23, 30], platinum [31–36], and palladium [34, 37–39]. The complexes of platinum group metals are most efficient, but are not the best choice due to their high cost. Redox-active heteroleptic complexes based on less expensive main group metals may prove to be efficient. Recently, absorption in the visible and near-IR spectral region corresponding to efficient intramolecular charge transfer between the donor ligand (catecholate or amidophenolate) and the acceptor ligand (2,2'-bipyridine) was observed for gallium(III) complexes with a distorted square pyramidal geometry [40, 41]. Meanwhile, the octahedral geometry of the coordination unit involving the same ligand systems does not provide conditions for LL'CT [40, 42]. In continuation of these studies, here we synthesized new zinc catecholate complexes with 2,2'-bipyridine (Bipy) and phenanthroline (Phen) and studied their electronic spectra.

EXPERIMENTAL

All operations for the synthesis and reactivity studies of zinc complexes were carried out in the absence of oxygen and air moisture. The solvents used in the study were purified and dehydrated as recommended in the literature [43]. Commercially available Zn (metal) (Aldrich), Bipy (Aldrich), and Phen (Aldrich) were used. 3,6-Di-*tert*-butyl-*o*-benzoquinone was synthesized by a reported procedure [44]. Infrared spectra were recorded on a FSM-1201 FTIR spectrometer (mineral oil suspensions; KBr cells). Elemental analysis was carried out using an Elementar Vario El cube instrument. The electronic spectra of oil suspensions and solutions of the compounds were

Table 1. Crystallographic data, X-ray diffraction experiment and structure refinement details for **I** and **II**

Parameter	Value	
	$(\mathbf{I}\cdot THF)_2$	$(\mathbf{II}\cdot THF)_2$
Molecular formula	$C_{56}H_{72}N_4O_6Zn_2$	$C_{60}H_{72}N_4O_6Zn_2$
Crystal size, mm	0.280 × 0.130 × 0.050	0.170 × 0.060 × 0.050
System	Triclinic	Monoclinic
Space group	$P\bar{1}$	$C2/c$
a, Å	10.9193(6)	17.3053(6)
b, Å	15.1337(9)	22.7487(7)
c, Å	15.9563(9)	13.3755(5)
α, deg	83.681(2)	90
β, deg	83.994(2)	92.481(2)
γ, deg	74.934(2)	90
V, Å^3	2034.72(18)	5260.6(3)
Z	2	4
ρ(calcd.), g/cm^3	1.353	1.359
μ, mm^{-1}	1.005	0.968
θ_{min}–θ_{max}, deg	1.399–28.740	2.087–26.403
Number of measured reflections	42323	34267
Number of unique reflections	13071	5399
R_{int}	0.0442	0.0713
$S(F^2)$	1.035	1.024
R_1/wR_2 ($F^2 > 2\sigma(F^2)$)	0.0389/0.0955	0.0419/0.0902
R_1/wR_2 (for all reflections)	0.0540/0.1017	0.0659/0.1003
$\Delta\rho_{max}/\Delta\rho_{min}$, e/Å^3	1.016/–0.821	0.766/–0.456

measured on Carl Zeiss Jena Specord M400 and SF-2000 spectrometers, respectively.

Synthesis of (3,6-Cat)Zn·Bipy (I) and (3,6-Cat)Zn·Phen (II). Zinc catecholate with coordinated THF molecules (3,6-CatZn·2THF, where 3,6-Cat is 3,6-di-*tert*-butylcatecholate) was prepared by a reported procedure [45]. A solution of Bipy (0.312 g, 2 mmol) or Phen (0.36 g, 2 mmol) in THF was added to a light yellow solution of 3,6-CatZn·2THF (0.86 g, 2 mmol) in THF (1 : 1 reactant ratio). Mixing was carried out at 60°C and accompanied by the appearance of a dark burgundy (Bipy) or violet (Phen) color of the reaction mixture. Slow cooling of the solutions resulted in the precipitation of **I** and **II** as finely crystalline materials suitable for X-ray diffraction.

I: brown-red crystals; yield of 0.88 g (86%).

For $C_{56}H_{72}N_4O_6Zn_2$

Anal. calcd., %	C, 65.43	H, 7.06	N, 5.45
Found, %	C, 65.35	H, 6.92	N, 5.17

IR (ν, cm^{-1}): 1607 s, 1596 s, 1578 m, 1567 m, 1535 w, 1492 m, 1442 s, 1431 m, 1401 s, 1348 m, 1324 w, 1314 w, 1291 m, 1279 m, 1256 s, 1225 s, 1203 m, 1169 m, 1148 m, 1100 w, 1057 m, 1040 w, 1020 m, 970 s, 936 m, 922 m, 807 m, 783 m, 758 s, 735 s, 695 w, 677 m, 657 s, 628 w, 554 w, 535 w.

II: red-violet crystals; yield of 0.98 g (91%).

For $C_{60}H_{72}N_4O_6Zn_2$

Anal. calcd., %	C, 66.97	H, 6.74	N, 5.21
Found, %	C, 66.77	H, 7.01	N, 4.98

IR (ν, cm^{-1}): 1624 w, 1581 w, 1519 m, 1462 s, 1434 s, 1396 s, 1352 m, 1291 m, 1289 w, 1279 w, 1254 m, 1215 m, 1202 m, 1144 m, 1100 w, 967 m,

932 w, 922 w, 867 w, 845 s, 808 w, 770 m, 727 s, 698 w, 675 m, 648 m, 557 w, 536 w.

X-ray diffraction study of I and **II** was carried out on a Bruker D8 Venture Photon diffractometer (MoK_α, $\lambda = 0.71073$ Å, φ- and ω-scan modes, Incoatec IμS 3.0 microfocus X-ray source) at 100 K at the Center for Collective Use of Physical Investigation Methods of the Kurnakov Institute of General and Inorganic Chemistry, Russian Academy of Sciences. The primary indexing and refinement of the unit cell parameters and integration of the experimental reflection intensities were carried out using the Bruker APEX3 program package [46]. The absorption corrections were applied using the SADABS package [47]. The structures of **I** and **II** were solved by direct methods [48] and refined by full-matrix least-squares method on F^2 [49] in the anisotropic approximation for all non-hydrogen atoms without any constraints on the thermal or geometric parameters. The hydrogen atoms were placed into the calculated positions and refined in the riding model with $U_{iso}(H) = 1.5U_{eq}(C)$ for methyl hydrogen atoms and $1.2U_{eq}(O)$ for all other hydrogen atoms. The calculations were carried out using the SHELXTL program package [48, 49] in the OLEX2 structure visualization and analysis software [50]. The crystallographic data and X-ray diffraction experiment and structure refinement details are summarized in Table 1, and selected bond lengths are given in Table 2.

The structures were deposited with the Cambridge Crystallographic Data Centre (CCDC no. 2222704 (**I**), 2222705 (**II**); ccdc.cam.ac.uk/structures).

The calculations were carried out using the Gaussian 09 program [51] by the density functional theory (DFT) in the B3LYP/def2tzvp approximation. The stationary points were located by full geometry optimization for the molecular structures. The absence of imaginary frequencies indicates that the molecules are in potential energy minima. TD-DFT calculations for the optimized molecule **II** were carried out using the CAM-B3LYP functional [52], which proved to be efficient in the calculation of intramolecular charge transfer [53] with the 6-31G(d,p) functional.

RESULTS AND DISCUSSION

New zinc catecholates **I** and **II** with Bipy or Phen ligands in the metal coordination sphere were obtained by exchange of neutral ligands of known zinc 3,6-di-*tert*-butyl-catecholate containing metal-coordinated THF molecules [45] (Scheme 1). The reactants were mixed in THF at 60°C. Slow cooling of the obtained reaction mixture resulted in precipitation of **I** and **II** as fine red-brown and red-violet crystals suitable for X-ray diffraction.

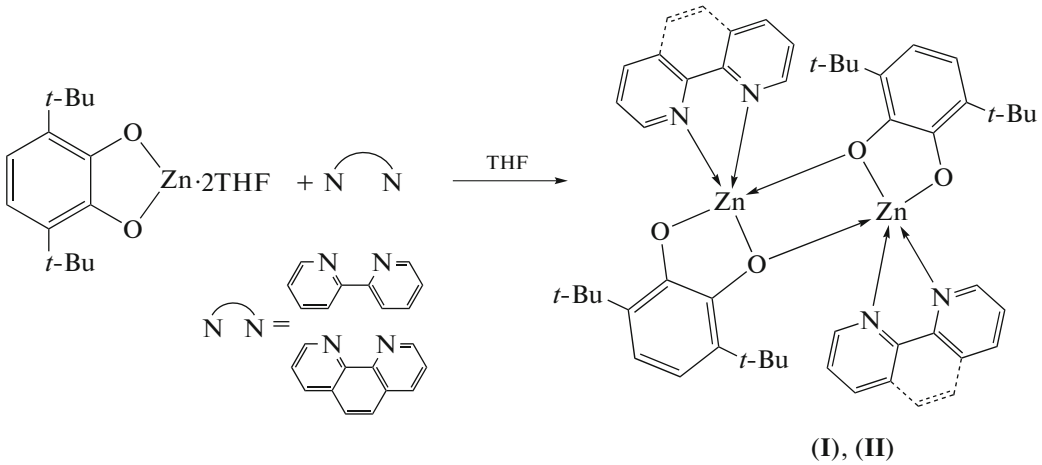

Scheme 1.

The molecular and crystal structures of complexes **I** and **II** were determined by X-ray diffraction study. The unit cell of **I** contains two independent zinc dimer molecules with similar structure. Therefore, only one of them is discussed below.

The molecules of complexes **I** and **II** have an inversion center and have a similar dimeric structure formed via pairwise coordination of one oxygen atom of the catecholate ligand to the neighboring zinc atom (Zn(1)–O(1A) and Zn(1A)–O(1) bond) (Fig. 1), like in the similar zinc complexes of a natural catechol, 4-methylesculetin, studied previously [54]. It is noteworthy that this type of oligomerization is rare for metal complexes based on 3,6-di-*tert*-butyl-*o*-benzoquinone, unlike the 3,5-substituted derivative [13]. Nevertheless, the bridging diolate coordination was noted in 3,6-di-*tert*-butylcatecholate complexes of main group metals such as magnesium [55], gallium [56], tin [57], and lead [58]. Complex **I** crystallizes in the triclinic space group $P\bar{1}$ as a solvate with a THF

Table 2. Selected bond lengths (Å) in complexes **I** and **II***

Bond	*d*, Å	
	I	**II**
Zn(1)–O(1)	2.0876(13)	2.1165(18)
Zn(1)–O(2)	1.9596(13)	1.9526(19)
Zn(1)–N(1)	2.1504(16)	2.180(2)
Zn(1)–N(2)	2.1323(16)	2.119(2)
Zn(1)–O(1A)	2.0147(14)	1.9867(19)
Zn(1)–Zn(1A)	2.8394(5)	2.8894(6)
Zn(2)–Zn(2B)	2.8911(4)	
O(1)–C(1)	1.375(2)	1.366(3)
O(2)–C(2)	1.338(2)	1.331(3)
Zn(1A)–O(1)	2.0147(14)	1.9867(19)
C(1)–C(2)	1.434(3)	1.441(4)
C(2)–C(3)	1.406(3)	1.407(4)
C(3)–C(4)	1.396(3)	1.394(4)
C(4)–C(5)	1.384(3)	1.394(4)
C(5)–C(6)	1.400(3)	1.396(4)
C(6)–C(1)	1.399(3)	1.395(4)

* Symmetry codes for the generation of equivalent atoms: (A) $-x+1$, $-y$, $-z+1$; (B) $-x+1$, $-y+1$, $-z$ (**I**). (A) $-x+3/2$, $-y+1/2$, $-z+1$; (B) $-x+1$, y, $-z+3/2$ (**II**).

molecule (3,6-Cat)Zn(Bipy)·2THF; thus, the unit cell contains one dimer complex molecule per two THF solvent molecules (Table 1). The composition of the unit cell of **II** is similar to that for **I**, (3,6-Cat)Zn(Phen)·2THF; however, **II** crystallizes in the monoclinic space group *C*2/*c* (Table 1). The zinc coordination polyhedron in both complexes is a distorted tetragonal pyramid, with two oxygen atoms of the catecholate ligand (O(1) and O(2)) and two 2,2'-bipyridine/phenanthroline nitrogen atoms (N(1) and N(2)) forming the base and the O(1A) oxygen atom of the neighboring *o*-quinone ligand being at the pyramid vertex. The planes forming the bases of both pyramids are parallel to each other (O(1), O(2), N(1), and N(2) lie in one plane and O(1A), O(2A), N(1A), and N(2A) are in the other plane). The planes of the catecholate and diimine ligands in the monomer units are located at 57.64° and 75.20° angles relative to each other in **I** and **II**, respectively. The Zn(1)O(1)Zn(1A)O(1A) quadrangle is a rhombus with Zn(1)O(1)Zn(1A) angles of 87.58° and 89.47° for **I** and **II**, respectively. The dimeric structure of **I** and **II** affects the bond length distribution in the coordination units. The Zn(1)–O(1) bonds between the metal and bridging oxygen atoms (2.0876(13) and 2.1165(18) Å for **I** and II, respectively) are longer than the bonds between Zn(1) and O(1A) atom of the neighboring catecholate ligand (2.0147(14) and 1.9867(19) Å for **I** and **II**, respectively). The Zn(1)–O(2) bonds are the shortest, being 1.9596(13) and 1.9526(19) Å long for **I** and **II**, respectively. Because of the bridging structure, the C–O bond lengths in each catecholate ligand are also non-equivalent. The C(1)–O(1) bonds (1.375(2) and 1.366(3) Å for **I** and **II**, respectively) are markedly longer than the C(2)–O(2) bonds (1.338(2) and 1.331(3) Å for **I** and **II**, respectively). The Zn–N distances are 2.1323(16) and 2.1504(16) Å for **I** and 2.119(2) and 2.180(2) Å for **II**, and are average values over the distances in known zinc *o*-quinone complexes with bidentate N-ligands [59]. The C–C bond lengths of *o*-quinone ligands are typical of metal catecholates [56, 60, 61].

In the crystals of **I** and **II**, a number of short contacts between aromatic moieties were found (Fig. 2). Some of them are classical π–π stacking interactions between the N-ligands of the neighboring dimers. These contacts are 3.532–3.586 Å long for **I** and 3.533–3.605 Å long for **II**. In turn, the C_{arom}–H...π type contacts provide additional intermolecular binding between dipyridyl (phenanthroline) ligands and catecholate moieties; their length is 3.614–3.795 Å for **I** and 3.672 Å for **II**.

The presence of quite a few short intermolecular contacts in crystalline samples of **I** and **II** determines their very low solubility in most available organic solvents. This precluded recording the NMR spectra for both complexes. Electronic absorption spectra for **II** were obtained in DMSO (Fig. 3). The observed spectrum exhibits a broad absorption band at 550 nm ($c = 5 \times 10^{-4}$ mol/L, $\varepsilon = 6.8 \times 10^2$ dm^3 mol^{-1} cm^{-1}), corresponding to π–π* transition and accounting for the observed violet color of the compound. The electronic spectra of a suspension of crystalline **I** and **II** were recorded in mineral oil (Fig. 3). Both crystalline samples show similar patterns of electronic spectra including a broad intense band in the visible region covering the edge of the near-IR region, 400–800 nm with a maximum at about 500 nm (Fig. 3).

The dimer complexes **I** and **II** and the monomer molecule of **I** were optimized by quantum chemical calculations using the DFT method at the B3LYP/def2tzvp level. The optimization of the four-coordinate monomer complex yields one stationary configuration with a highly distorted tetrahedral geometry of the coordination unit (Fig. 4).

The dihedral angle between the planes of the two bidentate ligands in the structure is 41.2°. In the geometry optimization, it is also possible to detect a square planar zinc catecholate molecule destabilized with respect to a distorted tetrahedron by 0.2 kcal/mol. However, the presence of one imaginary frequency for the planar structure indicates that it is a transition state. The dimer formation from two distorted tetrahedra stabilizes the system by 26.1 kcal/mol. This implies that dissociation of the dimer is unlikely at room tem-

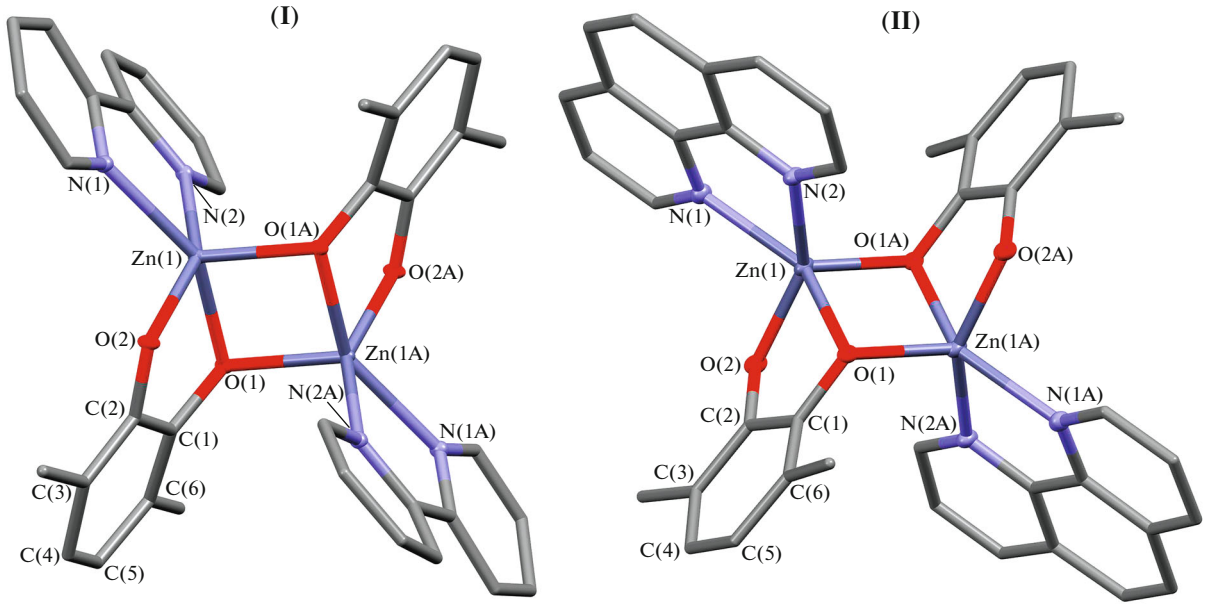

Fig. 1. Molecular structure of **I** and **II**. The thermal ellipsoids of particular atoms are given at 30% probability level. The hydrogen atoms, methyl groups of *t*-Bu, and solvation molecules of THF are omitted for clarity.

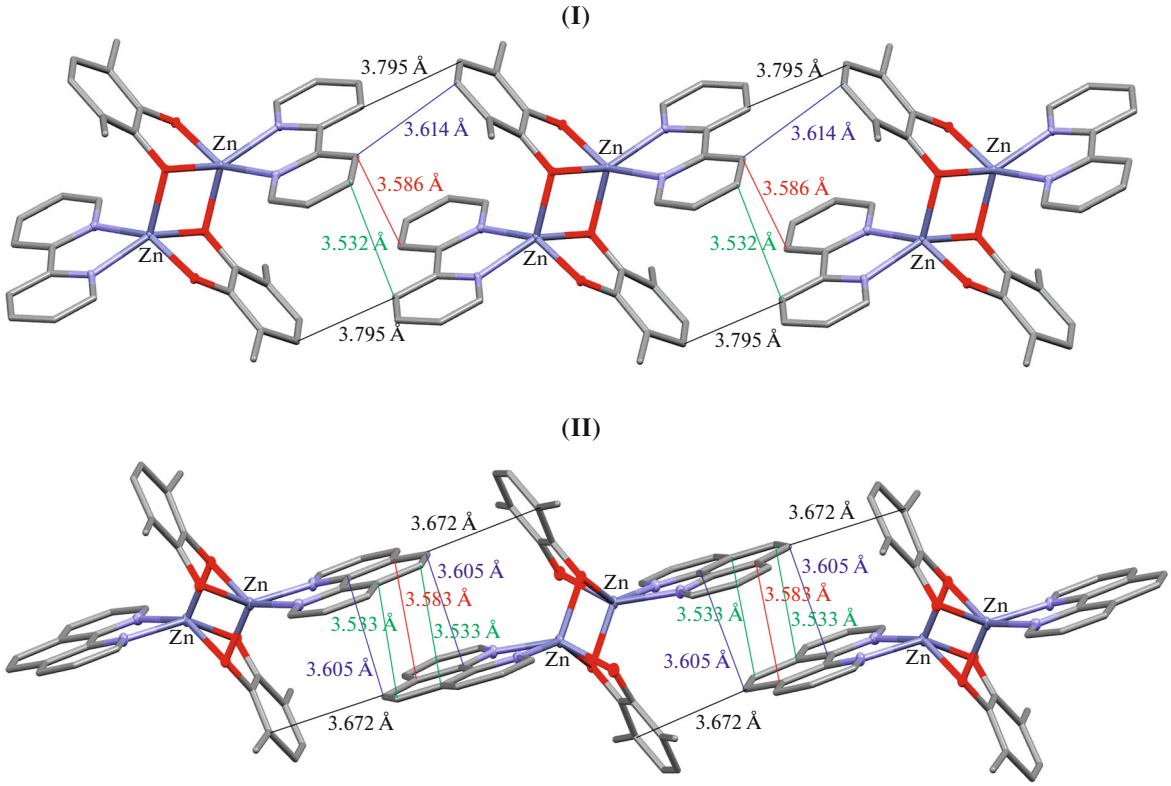

Fig. 2. Intermolecular contacts in **I** and **II**.

perature. The optimized geometry of dimers **I** and **II** adequately reproduces the structure derived from X-ray diffraction data. Molecular orbital analysis showed that the frontier orbitals are mainly located on the redox-active ligands. HOMO (–4.17 and –4.19 eV for **I** and **II**, respectively) and HOMO-1 (–4.20 and

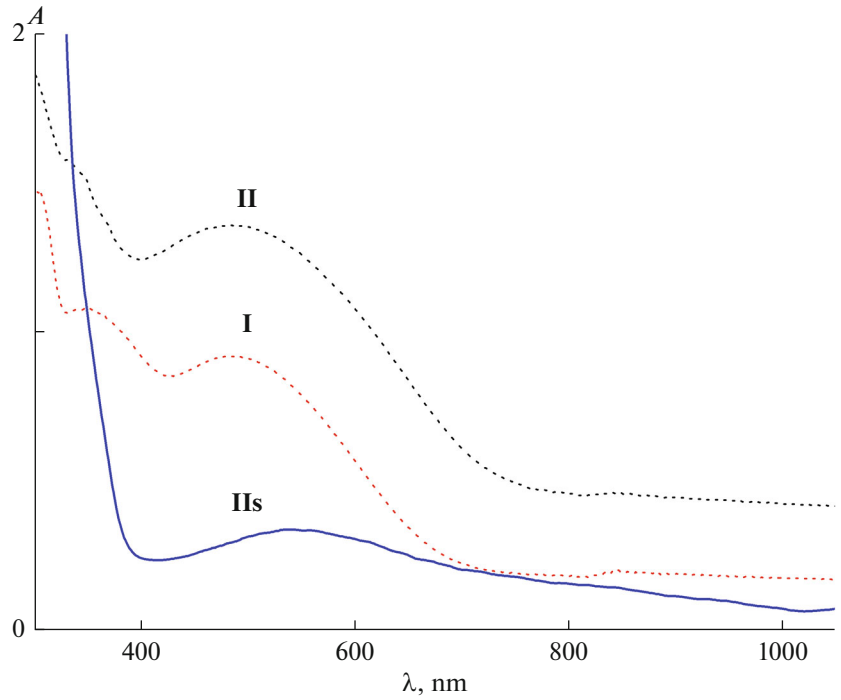

Fig. 3. Electronic absorption spectra of complexes **I** and **II**: the dashed lines designated as **I** and **II** correspond to the spectra of suspensions of crystalline **I** and **II** in mineral oil; the continuous line **IIs** is the spectrum of a solution of **II** in DMSO ($c = 5 \times 10^{-4}$ mol/L, $l = 1$ cm).

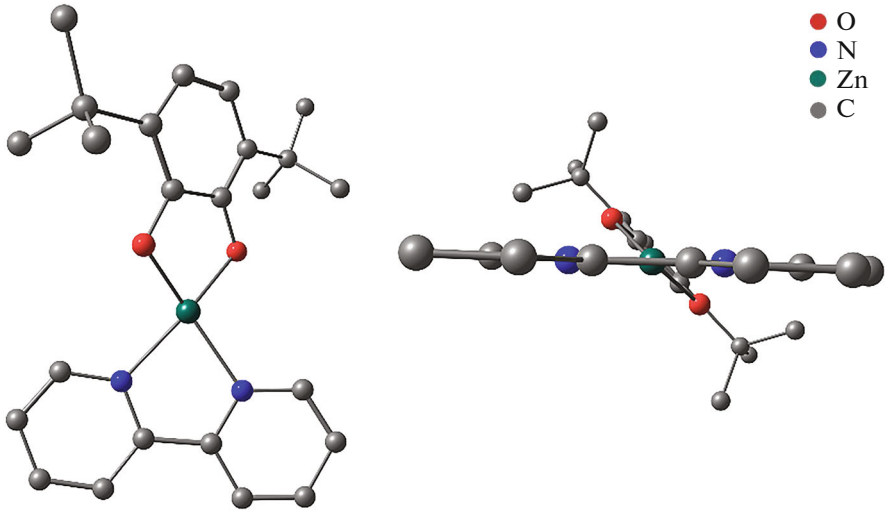

Fig. 4. Types of molecular structure of monomeric **I** derived from quantum chemical data.

−4.22 eV for **I** and **II**, respectively) are delocalized over the aromatic systems of the donor catecholate moiety (Fig. 5). HOMO has a small contribution of the zinc d_{xy} orbitals. LUMO (−2.51 and −2.52 eV for **I** and **II**, respectively) and LUMO+1 (−2.48 and −2.50 eV for **I** and **II**, respectively), which are nearly degenerate in energy, occupy the acceptor diimine ligands (Fig. 5).

According to TD-DFT data, the longest-wavelength absorption for the considered complexes is associated with two low-intensity transitions: HOMO−LUMO+1 (λ = 520.5 nm, 2.382 eV, oscillator strength of 0.0014 and λ = 523.8 nm, 2.367 eV, oscillator strength of 0.0019 for **I** and **II**, respectively) and HOMO-1−LUMO (λ = 508.5 nm, 2.430 eV,

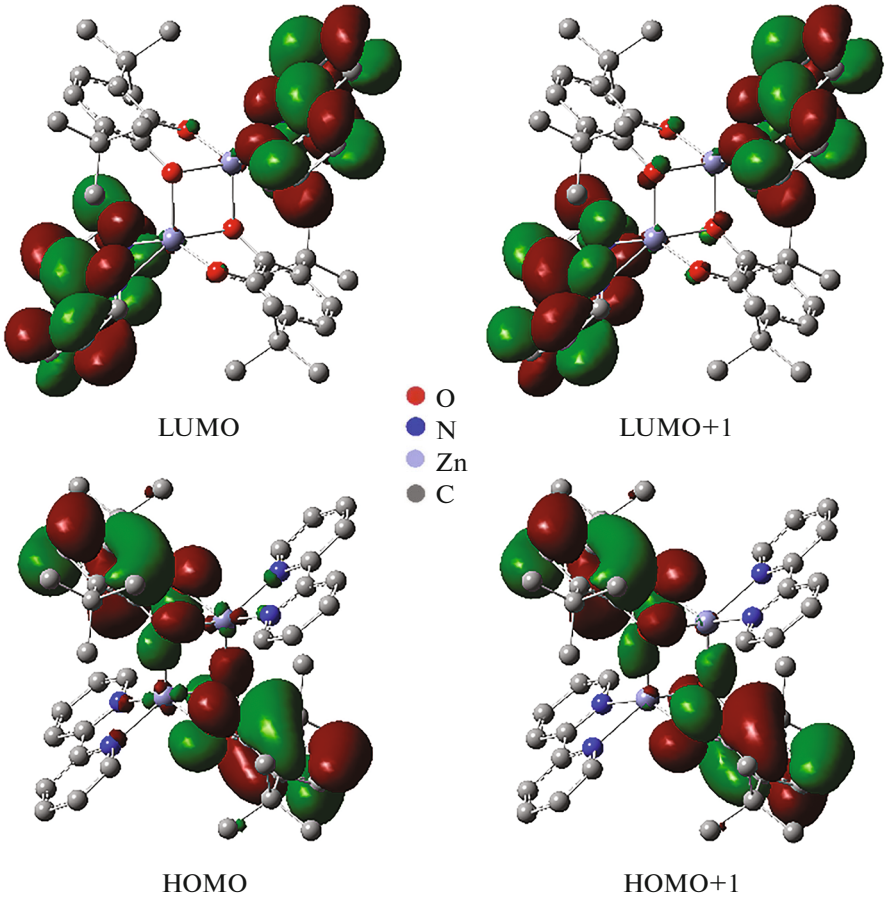

Fig. 5. Types of frontier orbitals of complex **I** according to quantum chemical data.

oscillator strength of 0.0252 and λ = 506.0 nm, 2.450 eV, oscillator strength of 0.0239 for **I** and **II**, respectively), which is in line with broad absorption bands at approximately 500 nm present in the electronic spectra of suspensions and DMSO solution (λ_{max} = 550.0 nm, 2.25 eV) of complex **II**. Thus, the observed color of complexes **I** and **II** is due to intramolecular ligand–ligand charge transfer between the catechol donor and the diimine acceptor. The presence of numerous close contacts between the molecules in the crystal packing of the compounds brings about additional possibilities for the intermolecular charge transfer; this changes the spectral characteristics of crystalline samples and produces a deeper color. It is noteworthy that attempts to observe LL'CT in similar centrosymmetric dimer zinc dithiolate complexes with bipyridine and phentanthroline have been already made previously [62]. The geometrical positions of the donor and acceptor redox-active ligands in the studied [62] five-coordinate zinc dithiolate derivatives should ensure more appropriate conditions for effective charge transfer: the dihedral angle between dithiolate and phenanthroline is 15.4°, which is much smaller than that in **I** or **II** (57.64° and 75.20°, respectively). Nevertheless, the authors were unable to observe the absorption bands corresponding to LL'CT in the electronic spectrum.

Thus, in this study, we synthesized new heteroleptic zinc 3,6-di-*tert*-butylcatecholate complexes with bidentately coordinated bipyridine or phenanthroline ligands. The compounds are dimerized through intermolecular Zn–O bonds. It was shown that both complexes exhibit absorption bands in the visible region corresponding to LLCT and caused by the presence of two oppositely charged redox-active ligands, donor catecholate ligand and acceptor diimine ligand.

ACKNOWLEDGMENTS

This study was performed using the equipment of the Center for Collective Use, Analytical Center of the Razuvaev Institute of Organometallic Chemistry, Russian Academy of Sciences, supported by the grant "Provision of the Development of the Material and Technical Infrastructure of the Centers for the Collective Use of Research Equipment" (unique identifier RF–2296.61321X0017, contract no. 075-15-2021-670). X-ray diffraction study of complexes **I** and **II** was carried out using the equipment of the Center for Collective Use of Physical Investigation Methods of the

Kurnakov Institute of General and Inorganic Chemistry, Russian Academy of Sciences.

FUNDING

This study was supported by the Russian Science Foundation (grant no. 22-13-00351).

CONFLICT OF INTEREST

The authors declare that they have no conflicts of interest.

REFERENCES

1. Weinstein, J.A., Tierney, M.T., Davies, E.S., et al., *Inorg. Chem.*, 2006, vol. 45, p. 4544.
2. Lu, X., Lee, S., Hong, Y., et al., *J. Am. Chem. Soc.*, 2017, vol. 139, p. 13173.
3. Cai, K., Xie, J., and Zhao, D., *J. Am. Chem. Soc.*, 2014, vol. 136, p. 28.
4. Pan, Z., Zhao, K., Wang, J., et al., *ACS Nano*, 2013, vol. 7, p. 5215.
5. Cui, B.-B., Zhong, Y.-W., and Yao, J., *J. Am. Chem. Soc.*, 2015, vol. 137, p. 4058.
6. Cui, B.-B., Tang, J.-H., Yao, J., et al., *Angew. Chem. Int. Ed.*, 2015, vol. 54, p. 9192.
7. Cameron, L.A., Ziller, J.W., and Heyduk, A.F., *Chem. Sci.*, 2016, vol. 7, p. 1807.
8. Espa, D., Pilia, L., Marchio, L., et al., *Dalton Trans.*, 2013, vol. 42, p. 12429.
9. Liu, Y., Zhang, Z., Chen, X., et al., *Dyes Pigments*, 2016, vol. 128, p. 179.
10. Wong, J.L., Higgins, R.F., Bhowmick, I., et al., *Chem. Sci.*, 2016, vol. 7, p. 1594.
11. Kramer, W.W., Cameron, L.A., Zarkesh, R.A., et al., *Inorg. Chem.*, 2014, vol. 53, p. 8825.
12. Ershova, I.V., Piskunov, A.V., and Cherkasov, V.K., *Russ. Chem. Rev.*, 2020, vol. 89, p. 1157.
13. Pierpont, C.G., *Coord. Chem. Rev.*, 2001, vols. 219–221, p. 415.
14. Abakumov, G.A., Piskunov, A.V., Cherkasov, V.K., et al., *Russ. Chem. Rev.*, 2018, vol. 87, p. 393.
15. Rajput, A., Sharma, A.K., Barman, S.K., et al., *Coord. Chem. Rev.*, 2020, vol. 414, p. 213240.
16. Pashanova, K.I., Poddel'sky, A.I., and Piskunov, A.V., *Coord. Chem. Rev.*, 2022, vol. 459, p. 214399.
17. Kaim, W., Das, A., Fiedler, J., et al., *Coord. Chem. Rev.*, 2020, vol. 404, p. 213114.
18. Dunn, T.J., Chiang, L., Ramogida, C.F., et al., *Chem.-Eur. J.*, 2013, vol. 19, p. 9606.
19. Chiang, L., Kochem, A., Jarjayes, O., et al., *Chem.-Eur. J.*, 2012, vol. 18, p. 14117.
20. Chiang, L., Herasymchuk, K., Thomas, F., et al., *Inorg. Chem.*, 2015, vol. 54, p. 5970.
21. Storr, T., Wasinger, E.C., Pratt, R.C., et al., *Angew. Chem. Int. Ed.*, 2007, vol. 46, p. 5198.
22. Kurahashi, T. and Fujii, H., *J. Am. Chem. Soc.*, 2011, vol. 133, p. 8307.
23. Aono, S., Nakagaki, M., Kurahashi, T., et al., *J. Chem. Theory Comput.*, 2014, vol. 10, p. 1062.
24. Kochem, A., Gellon, G., Leconte, N., et al., *Chem.-Eur. J.*, 2013, vol. 19, p. 16707.
25. Clarke, R.M., Jeen, T., Rigo, S., et al., *Chem. Sci.*, 2018, vol. 9, p. 1610.
26. Ward, M.D., *J. Solid State Electrochem.*, 2005, vol. 9, p. 778.
27. Pashanova, K.I., Bitkina, V.O., Yakushev, I.A., et al., *Molecules*, 2021, vol. 26, p. 4622.
28. Pashanova, K.I., Ershova, I.V., Trofimova, O.Y., et al., *Molecules*, 2022, vol. 27.
29. Clarke, R.M., Hazin, K., Thompson, J.R., et al., *Inorg. Chem.*, 2016, vol. 55, p. 762.
30. Lecarme, L., Chiang, L., Moutet, J., et al., *Dalton Trans.*, 2016, vol. 45, p. 16325.
31. Yang, J., Kersi, D.K., Giles, L.J., et al., *Inorg. Chem.*, 2014, vol. 5, p. 4791.
32. Rauth, G.K., Pal, S., Das, D., et al., *Polyhedron*, 2001, vol. 20, p. 363.
33. Heinze, K. and Reinhardt, S., *Chem.-Eur. J.*, 2008, vol. 14, p. 9482.
34. Deibel, N., Schweinfurth, D., Fiedler, J., et al., *Dalton Trans.*, 2011, vol. 40, p. 9925.
35. Scattergood, P.A., Jesus, P., Adams, H., et al., *Dalton Trans.*, 2015, vol. 44, p. 11705.
36. Best, J., Sazanovich, I.V., Adams, H., et al., *Inorg. Chem.*, 2010, vol. 49, p. 10041.
37. Roy, R., Chattopadhyay, P., and Sinha, C., *Polyhedron*, 1996, vol. 15, p. 3361.
38. Tahara, K., Kadowaki, T., Kikuchi, J., et al., *Bull. Chem. Soc. Jpn.*, 2018, vol. 91, p. 1630.
39. Sobottka, S., Noßler, M., Ostericher, A.L., et al., *Chem.-Eur. J.*, 2020, vol. 26, p. 1314.
40. Maleeva, A.V., Ershova, I.V., Trofimova, O.Y., et al., *Mendeleev Commun.*, 2022, vol. 32, p. 83.
41. Ershova, I.V., Maleeva, A.V., Aysin, I.A., et al., *Russ. Chem. Bull.*, 2023, vol. 72, p. 193.
42. Maleeva, A.V., Trofimova, O.Y., Ershova, I.V., et al., *Russ. Chem. Bull.*, 2022, vol. 71, p. 1441.
43. Perrin, D.D., Armarego, W.L.F., and Perrin, D.R., *Purification of Laboratory Chemicals*, Oxford: Pergamon, 1980, p. 544.
44. Garnov, V.A., Nevodchikov, V.I., Abakumova, L.G., et al., *Bull. Acad. Sci. USSR*, 1987, vol. 36, p. 1728.
45. Piskunov, A.V., Maleeva, A.V., Abakumov, G.A., et al., *Russ. J. Coord. Chem.*, 2011, vol. 37, p. 243.
46. *APEX3, SAINT and SADABS,* Madison: Bruker AXS Inc., 2016.
47. Krause, L., Herbst-Irmer, R., Sheldrick, G.M., et al., *J. Appl. Crystallogr.*, 2015, vol. 48, p. 3.
48. Sheldrick, G.M., *Acta Crystallogr., Sect. A: Found. Adv.*, 2015, vol. 71, p. 3.
49. Sheldrick, G.M., *Acta Crystallogr., Sect. C: Struct. Chem.*, 2015, vol. 71, p. 3.
50. Dolomanov, O.V., Bourhis, L.J., Gildea, R.J., et al., *J. Appl. Crystallogr.*, 2009, vol. 42, p. 339.

51. Frisch, M.J., Trucks, G.W., Schlegel, H.B., et al., *Gaussian 09*, Wallingford (CT): Revision D.01. Inc., 2013.

52. Yanai, T., Tew, D.P., and Handy, N.C., *Chem. Phys. Lett.*, 2004, vol. 393, p. 51.

53. Loos, P., Comin, M., Blase, X., and Jacquemin, D., *J. Chem. Theory Comput.*, 2021, p. 3666.

54. Butler, I.S., Gilson, D.F.R., Jean-Claude, B.J., et al., *Inorg. Chim. Acta*, 2014, vol. 423, p. 132.

55. Piskunov, A.V., Lado, A.V., Abakumov, G.A., et al., *Russ. Chem. Bull.*, 2007, vol. 56, p. 97.

56. Piskunov, A.V., Maleeva, A.V., Mescheryakova, I.N., et al., *Eur. J. Inorg. Chem.*, 2012, vol. 2012, p. 4318.

57. Piskunov, A.V., Lado, A.V., Fukin, G.K., et al., *Heteroatom. Chem.*, 2006, vol. 17, p. 481.

58. Abakumov, G.A., Cherkasov, V.K., Piskunov, A.V., et al., *Russ. Chem. Bull.*, 2006, vol. 55, p. 1146.

59. Piskunov, A.V., Maleeva, A.V., Bogomyakov, A.S., et al., *Polyhedron*, 2015, vol. 102, p. 715.

60. Chegerev, M.G., Piskunov, A.V., Maleeva, A.V., et al., *Eur. J. Inorg. Chem*., 2016, vol. 2016, p. 3813.

61. Brown, S.N., *Inorg. Chem.*, 2012, vol. 51, p. 1251.

62. Wang, Q.-H., Long, D.-L., Hu, H.-M., et al., *J. Coord. Chem.*, 2000, vol. 49, p. 201.

Translated by Z. Svitanko